RAA 2014 Vol. **14** No. **10**, 1289–1300 doi: 10.1088/1674–4527/14/10/008
http://www.raa-journal.org *http://www.iop.org/journals/raa*

***R**esearch in*
***A**stronomy and*
***A**strophysics*

Association of CMEs with solar surface activity during the rise and maximum phases of solar cycles 23 and 24 *

Peng-Xin Gao[1,2,3], Ting Li[2] and Jun Zhang[2]

[1] National Astronomical Observatories/Yunnan Observatories, Chinese Academy of Sciences, Kunming 650011, China; *gaopengxin@ynao.ac.cn*
[2] Key Laboratory of Solar Activity, National Astronomical Observatories, Chinese Academy of Sciences, Beijing 100012, China
[3] Key Laboratory of Dark Matter and Space Astronomy, Purple Mountain Observatory, Chinese Academy of Sciences, Nanjing 210008, China

Received 2014 February 1; accepted 2014 April 22

Abstract The cyclical behaviors of sunspots, flares and coronal mass ejections (CMEs) for 54 months from 2008 November to 2013 April after the onset of Solar Cycle (SC) 24 are compared, for the first time, with those of SC 23 from 1996 November to 2001 April. The results are summarized below. (i) During the maximum phase, the number of sunspots in SC 24 is significantly smaller than that for SC 23 and the number of flares in SC 24 is comparable to that of SC 23. (ii) The number of CMEs in SC 24 is larger than that in SC 23 and the speed of CMEs in SC 24 is smaller than that of SC 23 during the maximum phase. We individually survey all the CMEs (1647 CMEs) from 2010 June to 2011 June. A total of 161 CMEs associated with solar surface activity events can be identified. About 45% of CMEs are associated with quiescent prominence eruptions, 27% of CMEs only with solar flares, 19% of CMEs with both active-region prominence eruptions and solar flares, and 9% of CMEs only with active-region prominence eruptions. Comparing the association of the CMEs and their source regions in SC 24 with that in SC 23, we notice that the characteristics of source regions for CMEs during SC 24 may be different from those of SC 23.

Key words: Sun: coronal mass ejections (CMEs) — Sun: filaments, prominences — Sun: flares — sunspots

1 INTRODUCTION

Coronal mass ejections (CMEs) are the most spectacular phenomena associated with solar activities and are often accompanied by other solar surface activities, e.g. flares and filament disappearances/prominence eruptions (hereafter, we will refer to both of these as “prominence eruptions”). The study of the association of CMEs with other solar surface activities is important in understanding the initiation mechanism of CMEs and will provide insights into the physical links between solar activity and the solar magnetic field.

* Supported by the National Natural Science Foundation of China.

Subramanian & Dere (2001) surveyed CMEs from 1996 January to 1998 May and found that 41% of the CMEs analyzed are associated with active regions (ARs) without prominence eruptions, 44% are associated with eruptions of AR prominences, and 15% are associated with quiescent prominence eruptions. From 1997 to 1998, about 63% of the CMEs are related to ARs and 37% of CMEs are not related to any AR (Chen et al. 2011). Zhou et al. (2003) found that, from 1997 to 2001, 88% of the CMEs analyzed are associated with flares and 94% are associated with prominence eruptions. Among these CMEs, there are 79% that are associated with ARs and 21% originate outside ARs.

During Solar Cycle (SC) 23, the association of a CME with other solar surface activity has been extensively studied. But so far, the corresponding study is rather rare for the current SC 24. The solar activity in SC 24 is significantly lower than that in SC 23. Nielsen & Kjeldsen (2011) showed an accumulation of spotless days during SC 24, and found that the accumulation of spotless days in SC 24 is comparable to that of SC 5 near the Dalton minimum and to that of SCs 12, 14 and 15 near the modern minimum (Usoskin 2008). SC 24 should be at the valley of a Centennial Gleissberg Cycle (Feynman & Ruzmaikin 2011; Li et al. 2011).

Compared with SC 23, solar surface activity events are relatively less during SC 24. Thus, the source locations of CMEs are relatively easy to identify with little ambiguity. That is to say, SC 24 will give us a great opportunity to further study the association of a CME with other solar surface activity. In Section 2, we show a comparative study of the cyclical behaviors of sunspots, flares and CMEs for 54 months after the onsets of SCs 23 and 24. Section 3 presents the statistical results of CMEs associated with different solar surface activity from 2010 June to 2011 June. A summary and discussion are given in Section 4.

2 THE CYCLICAL BEHAVIORS OF SUNSPOTS, FLARES AND CMES

In the study, the CME data come from the Large Angle and Spectrometric Coronagraph Experiment (LASCO; Brueckner et al. 1995) onboard the *Solar and Heliospheric Observatory* (*SOHO*; Domingo et al. 1995). The Coordinated Data Analysis Workshop (CDAW) CME catalog[1] provides the most reliable list of CMEs recorded so far by *SOHO*/LASCO. For each CME event, the catalog gives angular width, linear speed and so on. The time sequences of flare and sunspot counts are derived from the lists of the National Geophysical Data Center (NGDC)[2]. NGDC also presents a table listing minima and maxima for numbers of sunspots in different cycles: the minimum level of solar activity between SCs 22 and 23 occurred in 1996 November and that between SCs 23 and 24 occurred in 2008 November. In this paper, we investigate the cyclical behaviors of sunspots, flares and CMEs for 54 months after the onsets of SCs 23 (from 1996 November to 2001 April) and 24 (from 2008 November to 2013 April).

The numbers of sunspots and CMEs as a function of time for 54 months after the onsets of SCs 23 and 24 are shown in Figure 1. It is apparent that the sunspot number of SC 24 is significantly smaller than that of SC 23, however, the number of CMEs in SC 24 is dramatically larger than that in SC 23.

As is known, the fraction of small CMEs (with angular width smaller than 50°) has increased since the declining phase of SC 23 due to the improvement in LASCO images. For a comparison of number of CMEs between SCs 23 and 24, we exclude all the small CMEs. Thus, Figure 1 also shows the number of CMEs with angular width larger than 50° changing with time for 54 months after the onsets of SCs 23 and 24. We can find that, from 34 months to 51 months after the onsets of SCs 23 (from 1999 August to 2001 January) and 24 (from 2011 August to 2013 January), the number of CMEs with angular width larger than 50° for SC 24 is larger than that of SC 23; in another time interval, the number of CMEs with angular width larger than 50° for SC 24 is smaller than that of SC 23.

[1] *http://cdaw.gsfc.nasa.gov/CME list/ index.html*

[2] *ftp://ftp.ngdc.noaa.gov/STP/space-weather/solar-data/*

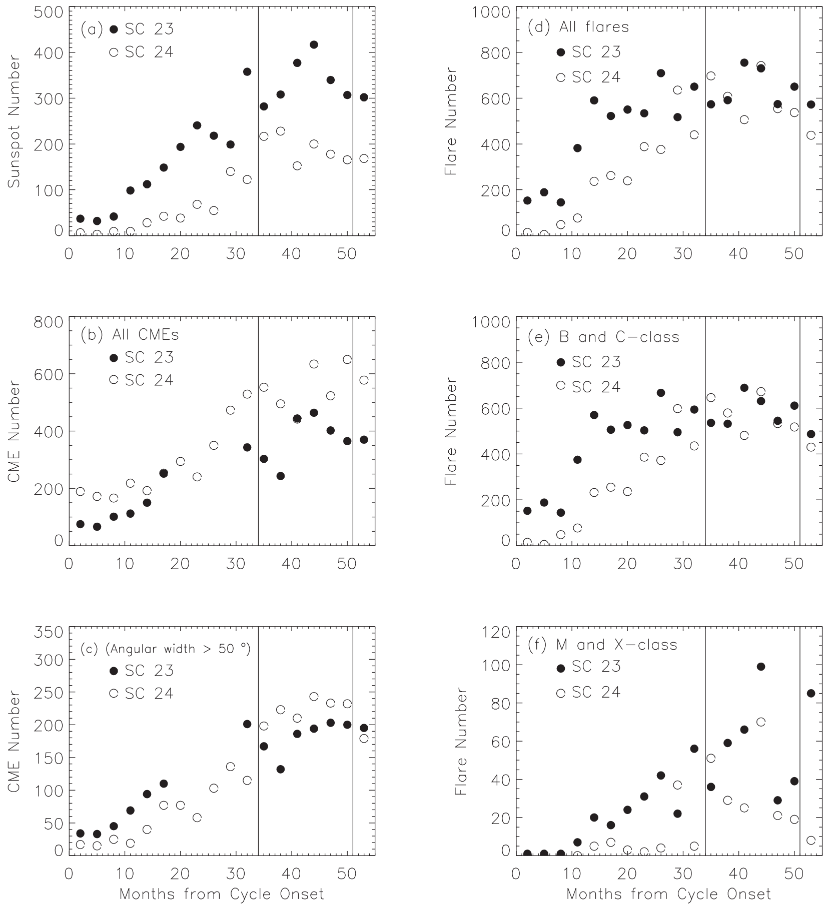

Fig. 1 The 3-monthly numbers of sunspots (a), CMEs (b), CMEs with angular width larger than 50° (c), flares (d), B- and C-class flares (e), and M- and X-class flares (f) for 54 months after the onsets of SCs 23 (*filled circles*) and 24 (*unfilled circles*). For the number of CMEs, there was a data gap of nine months due to interruption of the *SOHO* mission during the interval 1998 June to 1999 February. In each panel, the vertical line on the left side represents the Month from Cycle Onset = 34 and the vertical line on the right side represents the Month from Cycle Onset = 51.

In other words, during the maximum phase, the number of CMEs with angular width larger than 50° in SC 24 is larger than that in SC 23. Thus, we are also concerned with sunspots and CMEs during the maximum phase, i.e. from 34 to 51 months after the onsets of SCs 23 and 24. For SCs 23 and 24, the total number of sunspots during the maximum phase is 2029 and 1140, respectively, indicating that the total number of sunspots in SC 24 is about 56% of that in SC 23. For SC 24, the total number of CMEs is 3297, which is 1.48 times that (2221) of SC 23, and the total number of CMEs with angular width larger than 50° (1339) in SC 24 is 1.23 times that (1082) of SC 23.

We also plot the numbers of all flares, B- and C-class flares, and M- and X-class flares changing with time for 54 months after the onsets of SCs 23 and 24, as shown in Figure 1. During the maximum phase, the total number of flares and the total number of B- and C-class flares from SC 24 are 3644 and 3429, respectively, which are comparable to the numbers (3873 and 3544) from SC 23, however,

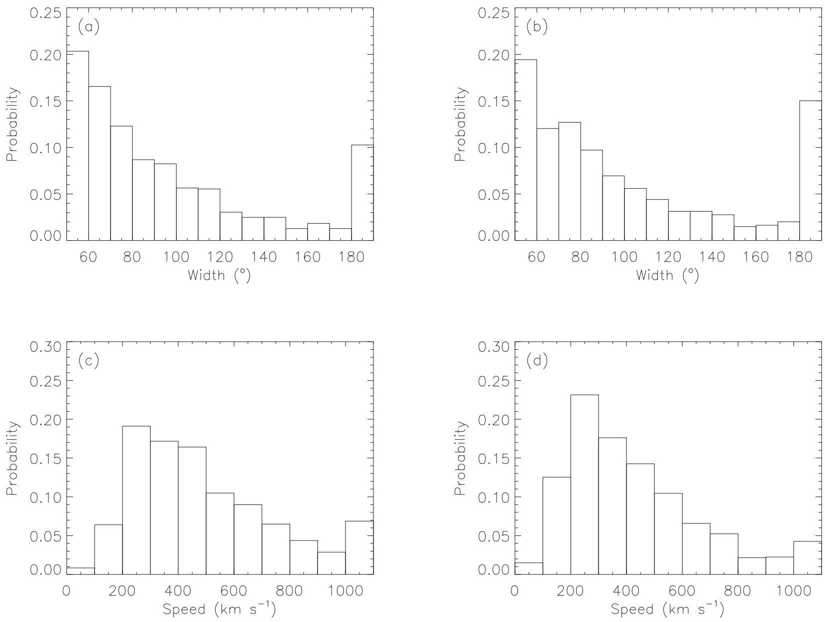

Fig. 2 The width and speed distributions of CMEs with angular width larger than 50° from 34 months to 51 months after the onsets of SCs 23 ((a) and (c)) and 24 ((b) and (d)). The CMEs with angular widths larger than 180° are put into the bin of 180°–190° and the CMEs with speeds higher than 1000 km s^{-1} in our sample are binned in the 1000 – 1100 km s^{-1} interval.

the total number of M- and X-class flares (328) from SC 24 is about 65% of that (215) from SC 23. In other time intervals, the number of flares from SC 24 is smaller than that from SC 23.

Figure 2 shows the speed and angular width distributions of CMEs with angular width larger than 50° from 34 months to 51 months after the onsets of SCs 23 and 24. The probabilities in terms of a bin size of 10° and 100 km s^{-1} are obtained by dividing the number of CMEs in each bin by the total number of CMEs. The CME events with angular widths larger than 180° in our sample are put into the bin of 180–190° and the CME events with speed larger than 1000 km s^{-1} in our sample are binned in the 1000–1100 km s^{-1} interval.

For CMEs with angular width larger than 50°, there are similar probabilities of CMEs with smaller angular widths in two cycles. However, the probabilities of CMEs in SC 24 with smaller speeds are higher than those in SC 23. We then calculate the mean angular widths and speeds of CMEs with angular width larger than 50° from 34 to 51 months after the onsets of SCs 23 and 24. For CMEs with angular width larger than 50°, the mean angular widths are 108° and 119°, respectively, indicating the mean angular width of SC 24 is 1.10 times that of SC 23. The mean speed of CMEs with angular width larger than 50° (442 km s^{-1}) during SC 24 is about 86% of that (509 km s^{-1}) during SC 23.

3 STATISTICAL RESULTS OF CMES ASSOCIATED WITH DIFFERENT SOLAR SURFACE ACTIVITIES FROM 2010 JUNE TO 2011 JUNE

3.1 Data Selection

In this paper, we identify the source regions of CMEs from 2010 June to 2011 June before the maximum of SC 24, during which the solar activity level is low. Thus, the source locations of CMEs can be identified with little ambiguity (Wang et al. 2011).

The Atmospheric Imaging Assembly (AIA; Lemen et al. 2012) onboard the *Solar Dynamics Observatory* (*SDO*; Pesnell et al. 2012) has been producing high-resolution, full-disk images of the Sun and the Hinode Flare Catalogue[3] (Watanabe et al. 2012) is used to identify the CMEs associated with flares. Moreover, observations from the *Solar-Terrestrial Relations Observatory* (*STEREO*; Kaiser et al. 2008) Extreme-Ultraviolet Imager (EUVI; Wuelser et al. 2004) have provided evidence to demonstrate that some CMEs occur on the back side, and these CMEs are not included in our analysis. To identify the source locations of CMEs, observations from these instruments are analyzed.

We examine LASCO running difference movies and AIA 304 Å movies to check whether CMEs are associated with solar surface activity (including prominence eruptions and flares above B1.0 class). The solar surface activities associated with a given CME are determined with the following three criteria. (1) Their locations on the solar disk are consistent with the ejection direction of the corresponding CME observed by LASCO. (2) They occur within the time window of $T \pm 40$ min, where T is the time of the CME initiation deduced by using the linear fit speed listed in the CME catalog. (3) Using *STEREO's* two-viewpoint observations, we exclude the CMEs whose surface activities are located at the farside of the Sun as seen from the perspective of *SDO*. In the process of identification, not all of the observations are good enough to identify the source locations of CMEs. In order to reduce uncertainties, we remove all the events whose identifications are ambiguous.

3.2 Result

From 2010 June to 2011 June, 1647 CMEs (445 CMEs with angular width larger than 50°) were observed by LASCO. Through individually examining the association between CMEs and solar surface activities, we identify 161 CMEs (88 CMEs with angular width larger than 50°) associated with solar surface activity.

In this paper, we identify 161 CMEs associated with prominence eruptions or flares, or 10% of all the 1647 CMEs observed by *SOHO*/LASCO. The percentage is less than those of Zhou et al. (2003) who found that 37% of CMEs (with angular width larger than 130°) analyzed are associated with filament eruptions or flares and Wang et al. (2011) who identified 26% of CMEs with locations identified on the front side of the solar disk. The fraction of small CMEs during SC 24 is larger than that during SC 23 due to the improvement in LASCO images. For CMEs with angular width larger than 50°, there are 20% of CMEs associated with prominence eruptions or flares, indicating that the CMEs with larger angular widths are relatively easier to identify than those with smaller angular widths. We may leave out the associated prominence eruptions or flares of some CMEs with small angular widths. This may be the reason why, in our sample, the percentage of CMEs associated with prominence eruptions or flares is less than those of Zhou et al. (2003) and Wang et al. (2011).

The 161 CME events are divided into the following four types: (1) associated with quiescent prominence eruptions (QP CMEs for short), (2) associated solely with AR prominence eruptions (AP CMEs for short), (3) associated with both AR prominence eruptions and flares (PF CMEs for short), and (4) associated solely with flares (FL CMEs for short). For an AP CME, there are no soft X-ray flares associated with this CME; for an FL CME, there are no prominence eruptions associated with this CME.

There are 73 (45%) QP CMEs, 44 (27%) FL CMEs, 30 (19%) PF CMEs and 14 (9%) AP CMEs. For the 73 QP CMEs, there are no soft X-ray flares which are associated with these prominence eruptions. Indeed, most of the prominence eruptions are accompanied by local brightening in the AIA images. However, these brightenings are too small to be termed flares. For CMEs with angular width larger than 50°, we can also obtain similar results. Nearly half of the CMEs are QP CMEs and their number is significantly larger than those of AP, PF and FL CMEs. All the sampled CMEs and associated surface activity are listed in Tables 1–4 (see online version).

[3] *http://st4a.stelab.nagoya-u.ac.jp/hinode_flare/*

Among these 161 CMEs, we select four well-observed CME events as examples to show the four types of CMEs. Figure 3 shows a CME event which is associated with a quiescent prominence eruption. The evolution of the erupting prominence is shown in Figure 3(a)–(b). The central location of this prominence is about N37E42. From the Helioseismic and Magnetic Imager (HMI; Schou & Larson 2011) line-of-sight magnetogram (Fig. 3(c)), we can find that this prominence is embedded in the quiet Sun and the magnetic field is weak; the magnetic flux of the footpoint of the prominence is 3.8×10^{20} Mx. The CME associated with the prominence eruption appeared in C2 at 07:12 UT. Then *SOHO*/LASCO observed the bright loop fronts of the CMEs at 08:24 UT. From the *SOHO*/LASCO image of the CME event (Fig. 3(d)), we can find that the bright leading edge of the CME filled the northeast quadrant.

The prominence began to rise at about 01:30 UT and attained the height of $\sim 1.3\ R_\odot$ at 05:58 UT, then, from 07:00 to 17:00 UT, the CME height gradually increased from about 3 $R_\odot$ to 17 $R_\odot$ (Fig. 3(e)). The speed of the prominence gradually increased and reached about 30 km s^{-1} at 05:58 UT. A fraction of this prominence is still observed by AIA at 06:50 UT and then left the AIA field-of-view. The prominence smoothly accelerates and reaches the speed of $\sim$ 90 km s^{-1} at 06:26 UT as observed by *STEREO B*. In the LASCO field-of-view, the CME speed gradually increased from $\sim$ 100 km s^{-1} to $\sim$ 400 km s^{-1} (Fig. 3(f)) and the average linear speed is 282 km s^{-1}.

A CME event only associated with the AR prominence eruption is shown in Figure 4. Figure 4(a) and (b) show the evolution of the prominence and the center of the prominence is located at N11W73. As is shown in Figure 4(c), this prominence was embedded in AR 11232 and this AR was in the decaying phase. *SOHO*/LASCO observed the CME associated with the prominence eruption after 14:48 UT and the bright loop fronts of the CME appeared in C2 at 15:24 UT. The *SOHO*/LASCO image of the CME event shows the bright leading edge of the CME filled the southwest quadrant (Fig. 4(d)).

From AIA 304 Å images, we notice that the height of the prominence increased from $\sim$ 1.1 $R_\odot$ to $\sim$ 1.3 $R_\odot$; at LASCO/C2 and C3, the CME height gradually increased and attained the height of $\sim$ 10 $R_\odot$ at 18:00 UT (Fig. 4(e)). At the end of the slow rise phase (about 14:18 UT), the prominence obtained a velocity of $\sim$ 100 km s^{-1}; then the speed quickly increased from $\sim$ 100 km s^{-1} to $\sim$ 200 km s^{-1} within $\sim$ 8 minutes (Fig. 4(f)). The speed of the CME decreased from $\sim$ 1000 km s^{-1} to $\sim$ 300 km s^{-1} within 4 hours (from 14:00 to 18:00 UT), as shown in Figure 4(f). The front traveled outward at an average linear speed of 493 km s^{-1}. Linear extrapolations of the height-time plots back to 1 $R_\odot$ show the CME was initiated at 13:54 UT.

The CME shown in Figure 5 is associated with both AR prominence eruption and a solar flare. The centers of the prominence and the M3.7 flare locations are N24W59 and N20W48, respectively, and they are located in the AR 11164 which was in the maximum phase, as shown in Figure 5(a) and (b). This flare started at 19:43 UT, peaked at 20:01 UT and ended at 20:12 UT. The first appearance of the associated CME in C2 was at 20:00 UT and the bright leading edge of the CME then filled the northwest quadrant.

The height of the prominence increased gradually and reached $\sim$ 1.05 $R_\odot$ at 19:42 UT, then its height quickly increased to $\sim$ 1.4 $R_\odot$ within $\sim$ 8 minutes. In the LASCO/C2 and C3 field-of-view, the CME height increased gradually from $\sim$ 2 $R_\odot$ to $\sim$ 25 $R_\odot$ from 19:30 to 22:30 UT (Fig. 5(e)). The speed of the prominence increased gradually and reached about 50 km s^{-1} at 19:42 UT, then the speed quickly increased to $\sim$ 700 km s^{-1} from 19:42 to 19:50 UT (Fig. 5(f)). The speed of the CME increased to $\sim$ 2500 km s^{-1} at $\sim$ 20:30 UT and then decreased to $\sim$ 1700 km s^{-1} at $\sim$ 22:00 UT (Fig. 5(f)). The evolutions of speed for the CME and prominence are synchronized in time with the *GOES* 1–8 Å soft X-ray flux profile (Fig. 5(f)). The speed as derived from a linear fit of the CME is 2125 km s^{-1} for the leading edge of the CME. Linear extrapolations of the height-time plots back to 1 $R_\odot$ show the CME was launched at 19:51 UT.

Figure 6 shows a CME only associated with a B5.7 flare. This flare started at 22:23 UT, peaked at 22:27 UT and ended at 22:30 UT and its location is N23W57. From the HMI line-of-sight magne-

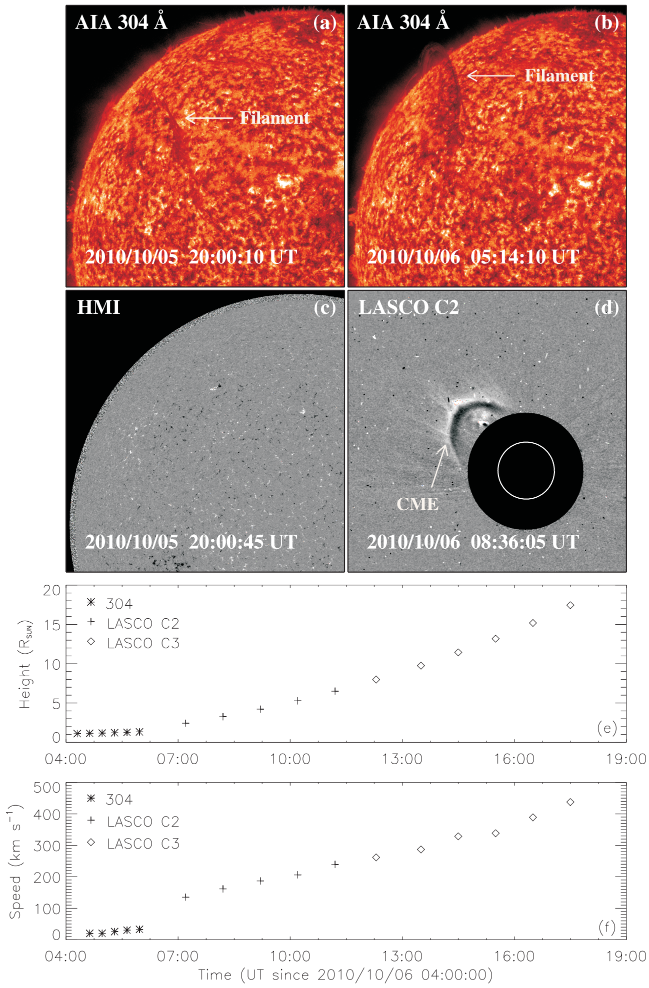

Fig. 3 Panels (a)–(b): *SDO*/AIA 304 Å images showing the evolution of a quiescent prominence from 2010 October 5 to 6; panel (c): HMI line-of-sight magnetogram at the location of the prominence; panel (d): *SOHO*/LASCO image of the CME associated with the prominence eruption; panels (e)–(f): height-time and velocity-time profiles of the prominence eruption at AIA 304 Å and the associated CME observed by LASCO/C2 and C3.

togram shown in Figure 6(c), we can find that this flare was located in the AR 11094. This AR was in the emerging phase. The CME associated with the solar flare was observed by *SOHO*/LASCO after 23:26 and its angular width was smaller than those of QP, AP and PF CME examples (Fig. 6(d)).

The CME height gradually increased from about 2 $R_\odot$ to 18 $R_\odot$ and the speed of the CME decreased from $\sim$ 400 km s^{-1} to $\sim$ 300 km s^{-1} from 00:00 to 08:00 UT, as shown in Figure 6(e) and (f). The average linear speed is 377 km s^{-1}. Linear extrapolations of the height-time plots back to 1 $R_\odot$ show the CME was initiated at 22:24 UT.

We then plot the speed distributions of QP, AP, PF and FL CMEs in Figure 7. The probabilities in terms of a bin size of 100 km s^{-1} are obtained by dividing the number of CMEs in each bin by the total number of CMEs. The CME events with a speed higher than 1000 km s^{-1} in our sample

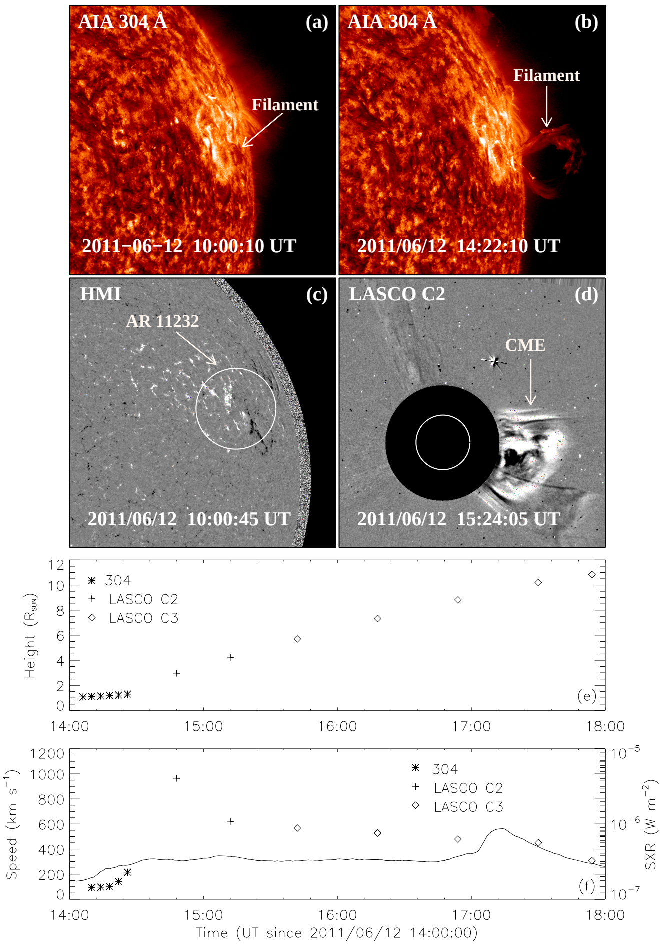

Fig. 4 Panels (a)–(b): *SDO*/AIA 304 Å images showing the evolution of an AR prominence on 2011 June 12; panel (c) HMI line-of-sight magnetogram at the location of the prominence; panel (d) *SOHO*/LASCO image of the CME associated with the prominence eruption; panels (e)–(f): height-time and velocity-time profiles of the prominence eruption at AIA 304 Å and the associated CME observed by LASCO/C2 and C3; the solid line in panel (f) denotes the *GOES* SXR 1–8 Å flux.

are binned in the 1000–1100 km s^{-1} interval. We calculate the mean speeds of QP, AP, PF and FL CMEs. For these four categories, the mean speeds are 369, 352, 617 and 418 km s^{-1}, respectively. QP and AP CMEs have quite similar mean speeds and are slightly slower than FL CMEs. The speed of PF CMEs is significantly larger than those of AP, QP and FL CMEs.

4 SUMMARY AND DISCUSSION

In this paper, we present a comparative study of the cyclical behaviors of sunspots, flares and CMEs for 54 months after the onsets of SCs 23 and 24 and find that the cyclical behavior of CMEs is different from those of sunspots or flares. Furthermore, during the maximum phase, the number of sunspots for SC 24 is significantly smaller than that for SC 23, however, the number of flares in SC 24 is comparable to that in SC 23. We find that, for the first time, the number of CMEs in SC 24 is

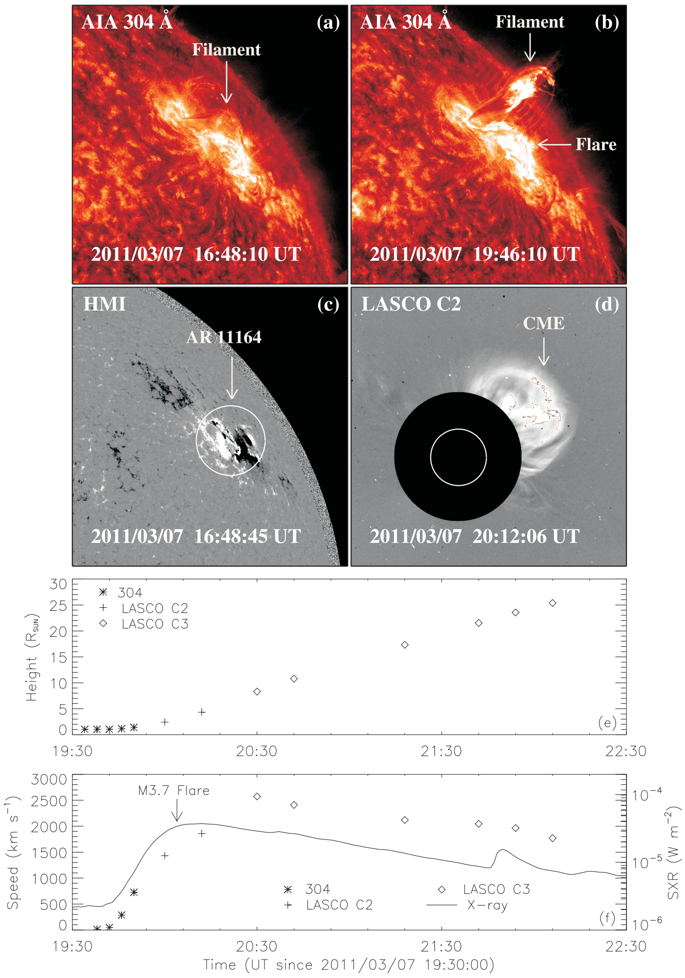

Fig. 5 Panels (a)–(b): *SDO*/AIA 304 Å images showing the evolution of an AR prominence and a flare on 2011 March 7; panel (c) HMI line-of-sight magnetogram at the AR location; panel (d) *SOHO*/LASCO image of the CME associated with both the prominence eruption and the flare; panels (e)–(f): height-time and velocity-time profiles of the prominence eruption at AIA 304 Å and the associated CME observed by LASCO/C2 and C3; the solid line in panel (f) denotes the *GOES* SXR 1–8 Å flux.

larger than that in SC 23 and the speed of CMEs in SC 24 is smaller than that in SC 23 during the maximum phase.

Based on *SOHO*/LASCO, *SDO*/AIA, HMI, *Hinode*, *STEREO* and other relevant observations, we identified 161 of 1647 CMEs observed by *SOHO*/LASCO during the period from 2010 June to 2011 June whose source regions are clearly observed on the solar disk and find that there are 45% QP CMEs, 27% FL CMEs, 19% PF CMEs and 9% AP CMEs. Their mean speeds are 369, 352, 617 and 418 km s^{-1}, respectively.

Nearly half of CMEs are associated with quiescent prominence eruptions. The percentage of occurrence for CMEs associated with activity on the solar surface in the quiet Sun is 1.21 times that of Chen et al. (2011), 2.14 times that of Zhou et al. (2003) and 3.00 times that of Subramanian &

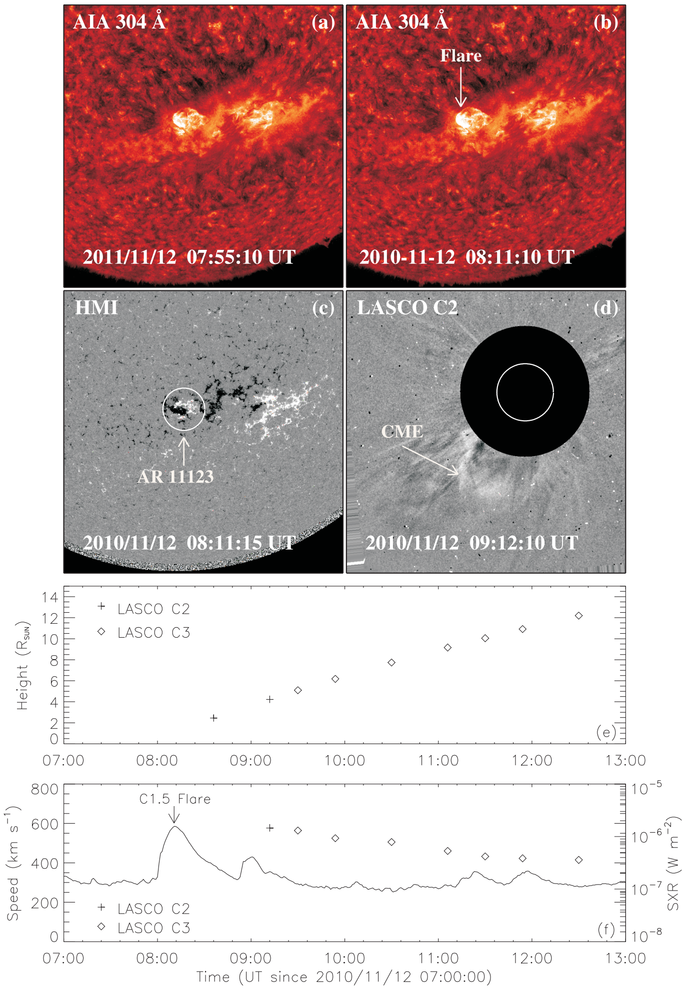

Fig. 6 Panels (a)–(b): *SDO*/AIA 304 Å images showing the evolution of a flare on 2010 August 5; panel (c) HMI line-of-sight magnetogram at the flare location; panel (d) *SOHO*/LASCO image of the CME associated with the flare; panels (e)–(f): height-time and velocity-time profiles of the associated CME observed by LASCO/C2 and C3; the solid line in panel (f) denotes the *GOES* SXR 1–8 Å flux.

Dere (2001) who studied CME events during SC 23. The criteria that are associated with activities on the solar surface associated with a given CME are similar to those employed by Zhou et al. (2003) and Chen et al. (2011). We conclude that, compared with SC 23, more CMEs originate from the quiet Sun during SC 24, suggesting that the characteristics of CME source regions during SC 24 may be different from those of SC 23.

Traditionally, there are two distinct types of CMEs, i.e. slow CMEs that are associated with prominence eruptions and fast CMEs that are associated with solar flares (Gosling et al. 1976; MacQueen & Fisher 1983; Sheeley et al. 1999; Moon et al. 2002). However, more and more evidence indicates that two types of CMEs have quite similar speed distributions (Vršnak et al. 2005; Chen et al. 2006). In our sample, the mean speed of CMEs only associated with prominence erup-

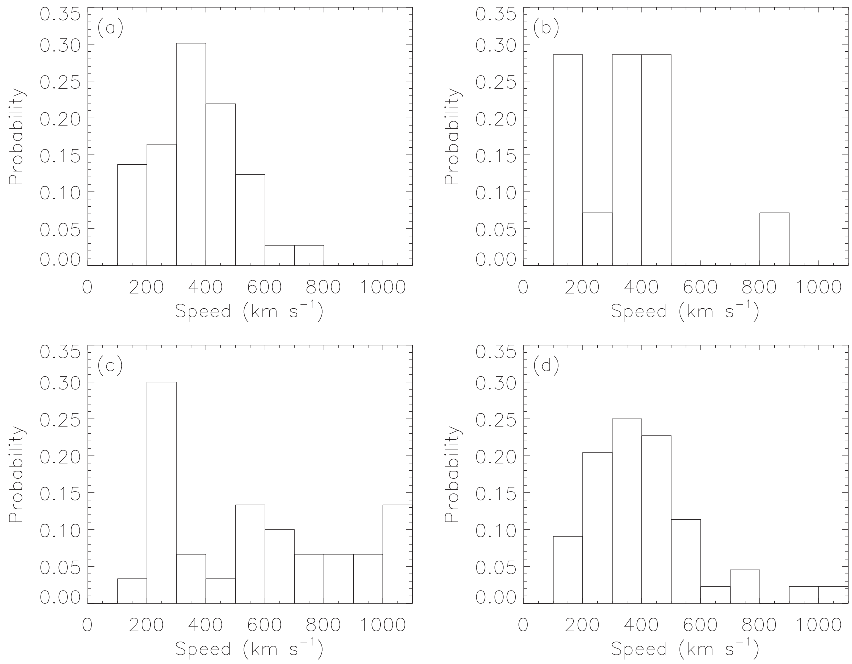

Fig. 7 The speed distributions of QP (a), AP (b), PF (c) and FL (d) CMEs. The CMEs with speeds higher than 1000 km s^{-1} in our sample are binned in the 1000 – 1100 km s^{-1} interval. The means in each panel are given.

tions (including QP and AP CMEs) is 366 km s^{-1} and the mean speed of CMEs only associated with flares (FL CME) is 418 km s^{-1}. The two types of CMEs include a comparable ratio of fast and slow CMEs, consistent with Vršnak et al. (2005). The speed of CMEs only associated with solar flares is slightly faster than that of CMEs only associated with prominence eruptions. A Kolmogorov-Smirnov test was performed on the speed distributions of the two types of CMEs and found that the P-value is 0.98 for the likelihood of the two distributions. The results are consistent with those of Chen et al. (2006) who also found that the mean speed of CMEs only associated with flares is slightly faster than that of CMEs only associated with prominence eruptions and the P-value is 0.79 for the likelihood of the speed distributions of the two types of CMEs. The two types of CMEs have quite similar speed distributions, with almost the same average speed. In terms of speed of CMEs, it is not certain that the CME should be classified as two physically distinct types according to the association with flares or prominence eruptions.

Moveover, we first find that, during the maximum phase, SC 24 has more CMEs than SC 23. However, the speeds of CMEs in SC 24 are smaller than those in SC 23. It is difficult to understand these behaviors. We speculate that the magnetic field of SC 24 is weak, thus the constraint on the background magnetic fields for the eruptive events should also be weak, which makes it easier for the CMEs to escape outward. The weak constraint of the background magnetic fields could also make it easier for small-scale eruptions to escape into the heliosphere. Recently, Hong et al. (2011) presented the first observations that the eruption of a mini-prominence in the quiet Sun was associated with a mini CME. A similar conclusion was drawn by Zheng et al. (2011), Yang et al. (2012) and Hong et al. (2013). This may explain why, in SC 24, the number of CMEs is larger than that in SC 23 and the speeds of CMEs are smaller than those of SC 23. A comprehensive understanding of these behaviors needs to be analyzed in further studies.

Acknowledgements We acknowledge the *SOHO*/LASCO, *SDO*/AIA, HMI and *STEREO* for providing data. The solar flare and sunspot listing used in this study were downloaded from NGDC. The authors express their deep thanks to the staff who maintain this website. The CME catalog is generated and maintained at the CDAW Data Center by NASA and The Catholic University of America in cooperation with the Naval Research Laboratory. *SOHO* is a project of international cooperation between ESA and NASA. This work was partly carried out by using the Hinode Flare Catalogue, which is maintained by ISAS/JAXA and the Solar-Terrestrial Environment Laboratory, Nagoya University. This work is supported by the National Natural Science Foundation of China (Grant Nos. 11203068, 11273057, 11303050 and 11025315), the National Basic Research Program of China (973 program, 2011CB811406 and 2012CB957801), the Chinese Academy of Sciences, the Foundation of Key Laboratory of Solar Activity of National Astronomical Observatories of Chinese Academy of Sciences (KLSA201302), and the Key Laboratory of Dark Matter and Space Astronomy of Purple Mountain Observatory of Chinese Academy of Sciences (DMS2012KT008).

References

Brueckner, G. E., Howard, R. A., Koomen, M. J., et al. 1995, Sol. Phys., 162, 357
Chen, A. Q., Chen, P. F., & Fang, C. 2006, A&A, 456, 1153
Chen, C., Wang, Y., Shen, C., et al. 2011, Journal of Geophysical Research (Space Physics), 116, A12108
Domingo, V., Fleck, B., & Poland, A. I. 1995, Sol. Phys., 162, 1
Feynman, J., & Ruzmaikin, A. 2011, Sol. Phys., 272, 351
Gosling, J. T., Hildner, E., MacQueen, R. M., et al. 1976, Sol. Phys., 48, 389
Hong, J., Jiang, Y., Zheng, R., et al. 2011, ApJ, 738, L20
Hong, J.-C., Jiang, Y.-C., Yang, J.-Y., et al. 2013, RAA (Research in Astronomy and Astrophysics), 13, 253
Kaiser, M. L., Kucera, T. A., Davila, J. M., et al. 2008, Space Sci. Rev., 136, 5
Lemen, J. R., Title, A. M., Akin, D. J., et al. 2012, Sol. Phys., 275, 17
Li, K. J., Feng, W., Liang, H. F., Zhan, L. S., & Gao, P. X. 2011, Annales Geophysicae, 29, 341
MacQueen, R. M., & Fisher, R. R. 1983, Sol. Phys., 89, 89
Moon, Y.-J., Choe, G. S., Wang, H., et al. 2002, ApJ, 581, 694
Nielsen, M. L., & Kjeldsen, H. 2011, Sol. Phys., 270, 385
Pesnell, W. D., Thompson, B. J., & Chamberlin, P. C. 2012, Sol. Phys., 275, 3
Schou, J., & Larson, T. P. 2011, in AAS/Solar Physics Division Abstracts #42, 1605
Sheeley, N. R., Walters, J. H., Wang, Y.-M., & Howard, R. A. 1999, J. Geophys. Res., 104, 24739
Subramanian, P., & Dere, K. P. 2001, ApJ, 561, 372
Usoskin, I. G. 2008, Living Reviews in Solar Physics, 5, 3
Vršnak, B., Sudar, D., & Ruždjak, D. 2005, A&A, 435, 1149
Wang, Y., Chen, C., Gui, B., et al. 2011, Journal of Geophysical Research (Space Physics), 116, A04104
Watanabe, K., Masuda, S., & Segawa, T. 2012, Sol. Phys., 279, 317
Wuelser, J.-P., Lemen, J. R., Tarbell, T. D., et al. 2004, in Society of Photo-Optical Instrumentation Engineers (SPIE) Conference Series, 5171, Telescopes and Instrumentation for Solar Astrophysics, eds. S. Fineschi, & M. A. Gummin, 111
Yang, J.-Y., Jiang, Y.-C., Yang, D., et al. 2012, RAA (Research in Astronomy and Astrophysics), 12, 300
Zheng, R., Jiang, Y., Hong, J., et al. 2011, ApJ, 739, L39
Zhou, G., Wang, J., & Cao, Z. 2003, A&A, 397, 1057

Table 1 List of QP CMEs and Associated Solar Surface Activities

No.	First in C2 (UT)	CPA/PA	Prominence Location
1	2010-06-01 20:58	135	S49E23
2	2010-07-03 09:32	67	N32E56
3	2010-07-17 07:31	36	N59E82
4	2010-08-01 23:18	56	N29E14
5	2010-08-17 07:36	29	N63E55
6	2010-09-07 10:24	235	S48W43
7	2010-09-07 16:12	97	N17E28
8	2010-09-08 17:12	128	S46E84
9	2010-09-11 02:00	65	N34E34
10	2010-09-12 07:24	136	S46E69
11	2010-09-15 12:48	309	N35W70
12	2010-09-16 13:36	311	N60W50
13	2010-09-19 02:48	341	N77W58
14	2010-09-22 16:24	330	N63W41
15	2010-09-28 16:12	261	N20W49
16	2010-09-29 10:12	30	N28E51
17	2010-09-30 23:05	358	N56W82
18	2010-10-06 07:12	6	N37E42
19	2010-10-07 07:24	294	N48w83
20	2010-10-10 18:00	41	N67E83
21	2010-10-16 04:13	312	N43W79
22	2010-10-26 10:12	318	N57W81
23	2010-11-17 02:24	318	N44W84
24	2010-11-24 07:36	327	N68W79
25	2010-11-30 19:12	72	N12E39
26	2010-12-03 19:00	322	N72W86
27	2010-12-06 17:24	125	S35E53
28	2010-12-10 06:48	283	N33W76
29	2010-12-11 16:00	223	S58W69
30	2010-12-12 05:00	21	N63E13
31	2010-12-16 08:48	321	N35W03
32	2010-12-21 02:48	48	N33E40
33	2010-12-22 03:12	338	N66W59
34	2010-12-23 11:00	127	S60E80
35	2010-12-24 05:00	263	S19W86
36	2010-12-25 11:12	255	S30W70
37	2010-12-25 13:48	83	N11E84
38	2010-12-25 14:48	263	S24W67
39	2010-12-30 09:36	283	N17W84
40	2011-01-24 02:00	260	S49W55
41	2011-01-28 05:00	116	S26E66
42	2011-01-30 18:36	281	N22W35
43	2011-02-02 07:36	302	N61W58
44	2011-02-05 00:00	282	N53W76
45	2011-02-10 13:48	108	S35E85
46	2011-02-11 17:48	337	N43W03
47	2011-02-25 20:24	300	N66W34
48	2011-02-26 14:12	332	N26W25
49	2011-02-27 10:48	82	N13E67
50	2011-03-02 02:24	231	S33W50
51	2011-03-03 20:57	78	N14E86
52	2011-03-04 05:36	89	S19E85
53	2011-03-19 21:24	110	S47E52
54	2011-03-23 01:36	21	N56E48
55	2011-03-24 04:36	136	S44E67
56	2011-03-29 18:12	11	N66E57
57	2011-04-09 14:24	234	S11W18
58	2011-04-11 22:36	277	N05W74
59	2011-04-15 00:24	86	S06E47
60	2011-04-18 23:24	63	N22E73
61	2011-04-24 14:36	322	N68W53
62	2011-05-17 04:36	331	N10W13
63	2011-05-21 01:25	123	S32E88
64	2011-05-23 03:48	13	N20E28
65	2011-05-26 19:12	359	N71E77
66	2011-06-05 03:44	18	N37W35
67	2011-06-06 07:30	241	S41W88
68	2011-06-09 19:36	22	N52E74
69	2011-06-12 15:48	292	N31W76
70	2011-06-14 18:36	319	N31W68
71	2011-06-23 09:48	107	N22E48
72	2011-06-24 19:48	116	S25E88
73	2011-06-28 05:00	202	S47E16

Table 2 List of FL CMEs and Associated Solar Surface Activities

No.	First in C2 (UT)	CPA/PA	Flare Grade	Flare Location	NOAA
1	2010-06-09 05:30	247	B5.1	S22W48	11078
2	2010-06-09 14:30	248	B2.1	S22W51	11078
3	2010-06-09 21:30	252	B2.7	S21W59	11078
4	2010-06-12 01:31	289	M2.0	N23W47	11081
5	2010-06-12 09:54	280	B2.4	N22W52	11081
6	2010-07-09 11:30	51	C1.8	N21E86	11087
7	2010-07-17 18:54	304	C2.4	N19W36	11087
8	2010-07-19 08:06	314	B5.5	N20W54	11087
9	2010-08-05 23:26	300	B5.7	N23W57	11094
10	2010-09-04 08:08	289	B6.0	N25W66	11103
11	2010-09-07 06:24	288	B4.4	N18W68	11105
12	2010-09-11 18:24	109	B3.6	S20E86	11106
13	2010-09-28 03:36	235	B2.3	S33W57	11108
14	2010-10-15 15:36	250	B1.4	S09W02	11112
15	2010-10-17 01:25	263	B4.5	S18W27	11112
16	2010-10-07 09:26	269	C1.7	S18W33	11112
17	2010-10-19 07:12	279	C1.3	S18W57	11112
18	2010-10-19 16:24	279	B3.2	S17W64	11112
19	2010-10-20 12:12	263	C1.5	S18W75	11112
20	2010-11-11 14:00	150	C2.2	S24E08	11123
21	2010-11-11 17:00	50	C4.3	S22E08	11123
22	2010-11-12 04:48	145	C1.0	S21E02	11123
23	2010-11-12 08:36	170	C1.5	S22E00	11123
24	2010-11-14 00:24	226	C1.1	S23W25	11123
25	2010-11-15 21:24	129	B4.5	S33E38	11126
26	2010-11-15 23:12	128	B8.3	S33E37	11126
27	2010-11-16 01:25	124	B4.5	S33E36	11126
28	2010-11-16 07:36	135	B3.6	S33E32	11126
29	2010-11-17 08:24	249	B3.4	S23W71	11123
30	2010-12-31 05:00	285	C1.3	N12W57	11138
31	2011-01-16 12:36	61	B1.5	N23E72	11147
32	2011-01-21 05:36	83	C3.3	N18E06	11149
33	2011-01-21 08:24	87	B9.5	N17E04	11149
34	2011-03-08 04:12	91	M1.5	S21E72	11171
35	2011-04-13 09:12	76	C1.2	N17E87	11191
36	2011-04-15 16:48	299	M1.3	N13W24	11190
37	2011-04-19 00:36	290	B7.6	N11W65	11190
38	2011-04-22 18:24	101	C5.5	S17E32	11195
39	2011-04-23 13:48	278	B8.1	N13W53	11193
40	2011-04-30 14:12	270	C3.2	S16W79	11195
41	2011-05-07 16:24	289	B3.3	N15W22	11203
42	2011-05-16 00:12	288	C4.8	N11W46	11208
43	2011-05-27 18:48	106	C1.1	S21E89	11226
44	2011-05-29 21:24	107	C8.7	S19E72	11227

Table 3 List of PF CMEs and Associated Solar Surface Activities

No.	First in C2 (UT)	CPA/PA	Flare Grade	Flare Location	Prominence Location	NOAA
1	2010-06-11 21:30	279	B4.5	N23W46	N22W44	11081
2	2010-08-07 18:36	94(PA)	M1.0	N14E37	N12E33	11093
3	2010-08-14 10:12	224(PA)	C4.4	N12W56	N13W63	11093
4	2010-09-04 15:12	270	B2.5	N22W87	N27W88	11102
5	2010-09-08 23:26	281	C3.3	N21W87	N23W89	11105
6	2010-09-22 04:24	88	B2.7	N20E78	N22E81	11109
7	2010-11-11 08:24	147	C4.7	S24E12	S23E07	11123
8	2010-11-15 15:48	221	B7.6	S22W43	S25W35	11123
9	2010-12-29 15:12	112	B1.2	S28E79	S26E83	11139
10	2011-01-26 16:00	280	B2.0	N14W72	N15W70	11149
11	2011-01-26 23:05	281	B3.2	N14W76	N14W73	11149
12	2011-01-27 07:36	292	B1.1	N15W88	N16W86	11149
13	2011-01-27 13:25	294	C1.2	N12W87	N15W87	11149
14	2011-01-28 01:25	288	M1.4	N16W88	N16W87	11149
15	2011-02-14 18:24	315(PA)	M2.2	S20W04	S19W02	11158
16	2011-02-15 02:24	189(PA)	X2.2	S20W10	S18W13	11158
17	2011-02-24 07:48	70	M3.5	N15E87	N18E88	11163
18	2011-02-25 06:12	74	C1.6	N27E85	N29E83	11163
19	2011-03-07 20:00	313	M3.7	N20W48	N24W59	11164
20	2011-03-08 20:12	236	M1.5	S19W87	S18W88	11165
21	2011-03-11 01:36	276	C1.4	N07W22	S14E39	11166
22	2011-04-12 13:25	105	C1.8	N09E88	N07E85	11191
23	2011-04-07 02:36	32	C2.0	N17E57	N16E45	11201
24	2011-05-11 02:48	320	B8.1	N19W51	N20W53	11204
25	2011-05-29 10:36	119	M1.4	S20E64	S17E57	11226
26	2011-06-01 17:36	93	C2.9	S21E16	E18E36	11226
27	2011-06-02 08:12	98	C2.2	S19E22	S20E12	11227
28	2011-06-06 06:45	289	B6.7	N19W25	N21W33	11228
29	2011-06-07 06:49	250	M2.5	S22W53	S23W58	11226
30	2011-06-11 09:36	290	B2.9	N20W89	N23W88	11230

Table 4 List of AP CMEs and Associated Solar Surface Activities

No.	First in C2 (UT)	CPA/PA	Prominence Location	NOAA
1	2010-07-09 20:54	48	N28E77	11087
2	2010-11-25 23:27	257	N23W37	11126
3	2010-12-01 04:48	82	N32E85	11131
4	2010-12-13 01:36	77	N25E88	11135
5	2011-02-16 02:36	51	N27E37	11160
6	2011-03-05 20:54	62	N22E87	11169
7	2011-03-10 22:24	83	N09E85	11172
8	2011-03-13 14:12	273	N07W61	11166
9	2011-03-27 05:36	54	N15E85	11183
10	2011-04-02 11:36	234	S25W23	11181
11	2011-04-24 09:24	62	N17E81	11201
12	2011-04-24 20:00	88	N17E88	11201
13	2011-05-04 17:48	55	N22E33	11205
14	2011-06-12 14:48	274	N11W73	11232